

Development of SAR Altimetry Mode Studies and Applications over Ocean, Coastal Zones and Inland Water (SAMOSA)

ESRIN Contract No. 20698/07/I-LG

WP8 Technical Note
Validation using airborne ASIRAS data

Version 1.0, July 6, 2009

Lars Stenseng
DTU-Space, National Space Institute
Juliane Maries Vej 30, DK-2100 Copenhagen O
Denmark

Contents

1	Introduction	1
2	ASIRAS (Airborne SAR/Interferometric Radar Altimeter System)	2
2.1	ASIRAS instrument	3
2.2	ASIRAS processor	4
3	CryoVEx 2006 campaign	6
3.1	Hardware Installation	7
4	ASIRAS HAM data over open ocean	9
4.1	Typical waveforms	9
4.1.1	Gaussian waveform	10
4.1.2	Skewed waveform	10
4.1.3	Waveform with tail	11
4.2	Distribution of typical waveforms	12
5	Waveform stacks before multi-look	14
5.1	Examples of stacks	14
5.2	Power versus look angle	14
6	Along-track beam selection	19
6.1	Comparison of full along-track beam summing and selected beam summing .	19
7	Guideline for future campaigns	22
8	Conclusion	23
	Reference	24

1 Introduction

The aim of the work presented in this technical note is to study and clarify the properties of data collected over the ocean with the ASIRAS instrument. Data acquired in high altitude mode over the Fram Strait, between Greenland and Svalbard, has been re-processed and is presented and analyzed using an empirically approach.

The work is divided into four tasks:

- Identify typical ASIRAS waveform types over ocean and characterize these waveforms (in terms of e.g. waveform width, return power, slope of leading edge and slope of trailing edge).
- Investigate the occurrence of identified typical waveform types.
- Rerun the ASIRAS processor to obtain stack data output and perform an empirical study of the relation between look angle and power contends (prior to multi-looking) for a few typical waveforms.
- Investigate the effect of along-track beam selection.
- Produce a guideline for future ASIRAS campaigns, to ensure the collection suitable datasets in the future.

This technical note will also give an brief introduction to the ASIRAS instrument and the ASIRAS processor, but leaves the more detailed description to the work referenced and the existing technical notes produced by the SAMOSA team.

2 ASIRAS (Airborne SAR/Interferometric Radar Altimeter System)

The SAR altimetry principle (Raney, 1998) introduced a combination of small footprint size and several equivalent looks. The high resolution and low speckle noise is features that are desirable when trying to detect small scale features like leads between ice floes. It was therefore proposed that this new altimeter type should be used to monitor the sea-ice from space. The proposal were accepted for further studies by ESA and the work on the SIRAL instrument (Wingham et al., 2006) for CryoSat began.

The final approval of the CryoSat mission implied that the properties of the new SAR/interferometric altimeter SIRAL needed to be investigated thoroughly to understand the signatures of the return pulses from ice covered surfaces. It was decided that an airborne SAR/interferometric altimeter should be build and used to investigate the nature of SAR altimeter pulses and to optimize the processing. To further support the understanding of the radar returns the airborne radar should be supported by scientist that performed various measurements of snow and ice properties beneath the aircraft.

The ASIRAS (Airborne SAR/Interferometric Altimeter System) instrument (Lentz et al., 2002; Mavrocordatos et al., 2004; RST, 2007) were finished in 2003 as a mean to collect the needed data for the investigation. ASIRAS were designed according to the same principle as SIRAL, but scaled in parameters to accommodate the differences between a space borne and an airborne system. (See Table 1.)

	SIRAL		ASIRAS	
	SAR mode	SARin mode	LAM	HAM
Along-track beam width ^a	1.0766°		10°	
Across-track beam width ^b	1.2016°		2.5°	
Interferometer baseline	–	1.172 m	–	0.76 m
Transmitted power	25 W		5 W	
Center frequency	13.575 GHz		13.5 GHz	
Transmitted bandwidth	350 MHz		1,000 MHz	100, 300, 500, 700, 1,000 MHz
Transmitted pulse length	49 ms		80 μ s	4, 5, 20, 25, 30, 35, 40, 45 μ s
Pulse repetition frequency	18.182 kHz		2, 2.5, 3 kHz	2.5, 3, 4, 5, 6, 7, 8, 9, 10, 11, 12, 13, 14, 15 kHz
Measurement range gate	0.46875 m		0.109787 m	0.08783 m ^c
Average platform velocity	7,389 m/s		67 m/s	
Average range to surface	717 km		200 – 1,500 m	1,100 – 10,000 m

^a3 dB antenna mainlobe half power beam width

^b3 dB antenna mainlobe half power beam width

^cUsing typical pulse length and bandwidth of 4 μ s and 1 GHz respectively.

Table 1: Comparison between ASIRAS and SIRAL instrument characteristics. Only SAR altimetry modes are considered.

2.1 ASIRAS instrument

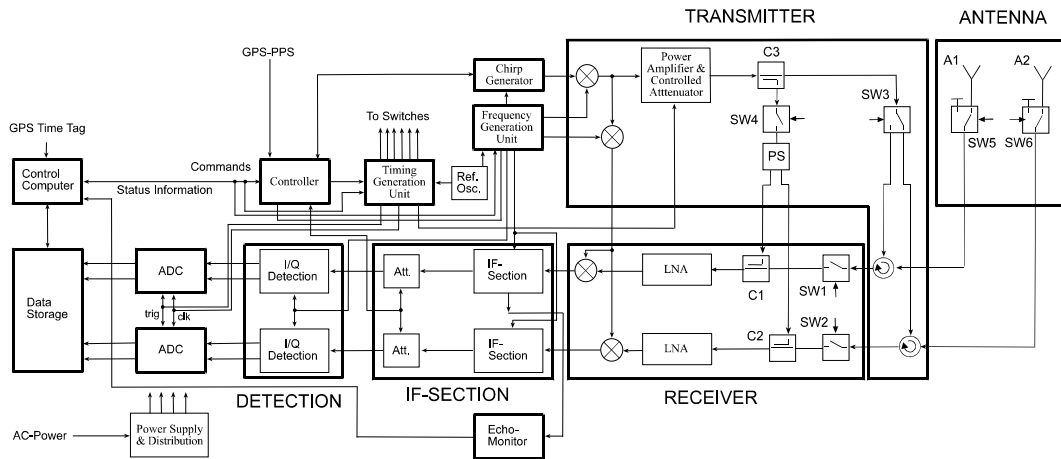


Figure 1: ASIRAS Hardware block diagram. (From RST (2007))

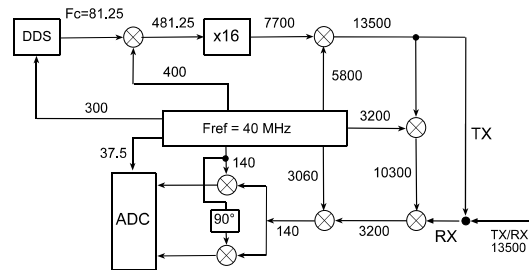


Figure 2: ASIRAS frequency plan (all frequencies are in MHz). (From RST (2007))

The ASIRAS instrument uses the deramp technique (MacArthur, 1976) to reduce the demands on data sampling and data volume needed to accommodate a 1 GHz bandwidth. Deramping is achieved by mixing the received signal with a time delayed replica of the transmitted linear FM signal which, after low pass filtering, removes the frequency ramp. For an ideal point target the deramped signal will be a single frequency pulse with a pulse length corresponding to the period where the delayed and the received signal overlap and a frequency proportional to the time shift between the replica signal and the received signal. To obtain a usable output the overlap between the replica and received signal needs to be of a certain size and the delay of the replica should therefore be optimized to best match the expected arrival of the received signal. For a real surface the deramped signal will consist of a whole spectrum of pulses with different frequencies and lengths. Since the replica and the received signal needs to overlap one can only observe objects within a certain range span which depends on the pulse length.

ASIRAS can be operated in two different modes; HAM (high altitude mode) 1,100 – 10,000 m above terrain and LAM (low altitude mode) 200 – 1,500 m. The HAM has two sub-modes SARIn and Enhanced SARIn both operating with one transmit/receive antenna and one receive antenna. In SARIn mode the signal is transmitted from one antenna and received with both antennas, thus enabling interferometry between the two

receiving antennas. The Enhanced SARIn mode is similar but the transmission is alternated from pulse to pulse between the two antennas.

The LAM were introduced in ASIRAS at a later stage to accommodate the coincident use of snow/ice laser scanners for collection of calibration and validation data. The short round-trip times associated with LAM requires very short pulses and replica delay times, but due the limitations on cpu time for signal generation it became undesirable to implement the deramping as described above, instead the concept of self-deramping is used. If the pulse length is significant longer than round-trip time it is possible to mix the transmitted pulse with the received signal while transmitting. In order to transmit while receiving it is necessary to use one antenna for transmitting and one antenna for receiving, this means that ASIRAS is unable to obtain interferometric data when operating in LAM.

Figure 1 shows a block diagram of the ASIRAS instrument. The GPS time tag and PPS (pulse per second) is fed into ASIRAS and used to tie the radar observations to the global UTC time frame. The frequency of the signal as it propagates through the different modules is described in figure 2. It should be noted that the 3,200 MHz and 3,060 MHz frequencies used to convert to the first and second IF-frequency can be varied when operating in LAM.

2.2 ASIRAS processor

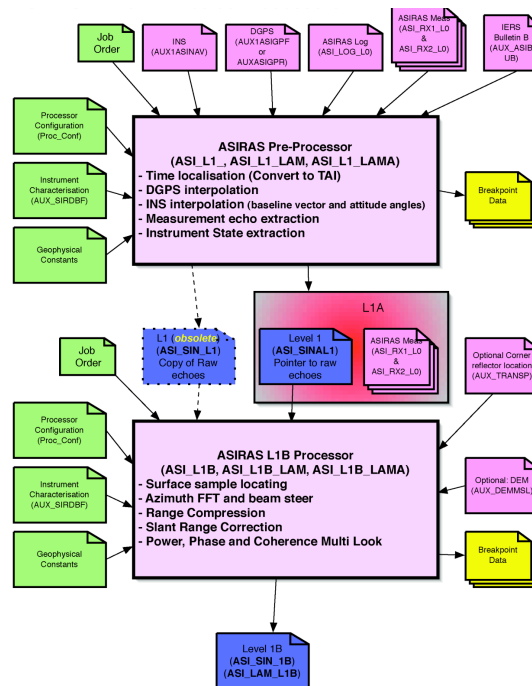


Figure 3: High level ASIRAS processor diagram. (From Cullen (2007))

The ASIRAS processor is a re-build of the CryoSat level 1b processor (Cullen and Wingham, 2002; ESA, 2007) that accounts for the differences between the space borne and the airborne instrument.

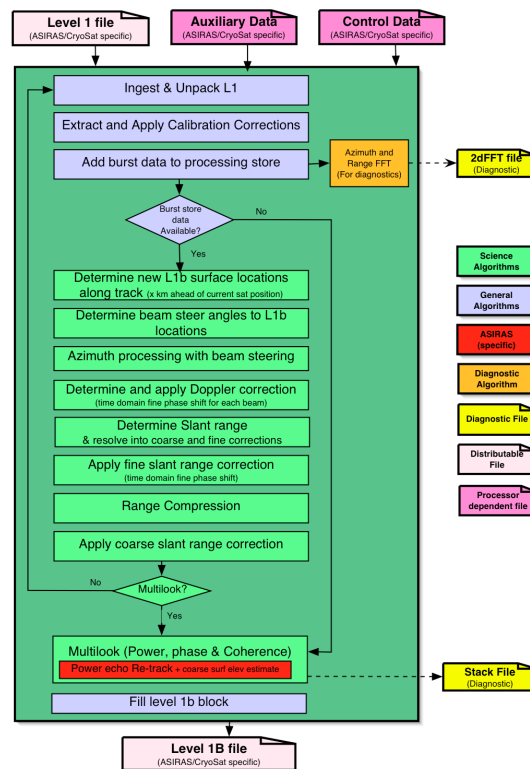


Figure 4: High level ASIRAS processor diagram. (From Cullen (2007))

The processing from level 0 to level 1b is performed in two steps, see figure 3. In the pre-processor the radar signals is combined with information on aircraft position and orientation and meta data regarding instrument parameters.

The science algorithms, see figure 4, implemented in the level 1b processor are similar to the ones used for CryoSat but modified for the different geometry and dynamics. The level 1b processor splits each echo into a set of Doppler beams illuminating a set of areas on the surface. All beams that illuminate a selected area on the surface are slant-range corrected¹ and summed to produce a level 1b waveform for the selected area. From the level 1b processor is possible to get various diagnostic output for example the stack file, which contains the individual beams before multilooking. The ASIRAS processor also performs a retracking of the multilooked power waveform using the OCOG (offset center of gravity) retracker. This retracking is purely for diagnostic purposes and only useful as a coarse indication of the range to the scattering surface.

¹Delay compensation and range migration are other often used terms for slant-range correction.

3 CryoVEx 2006 campaign

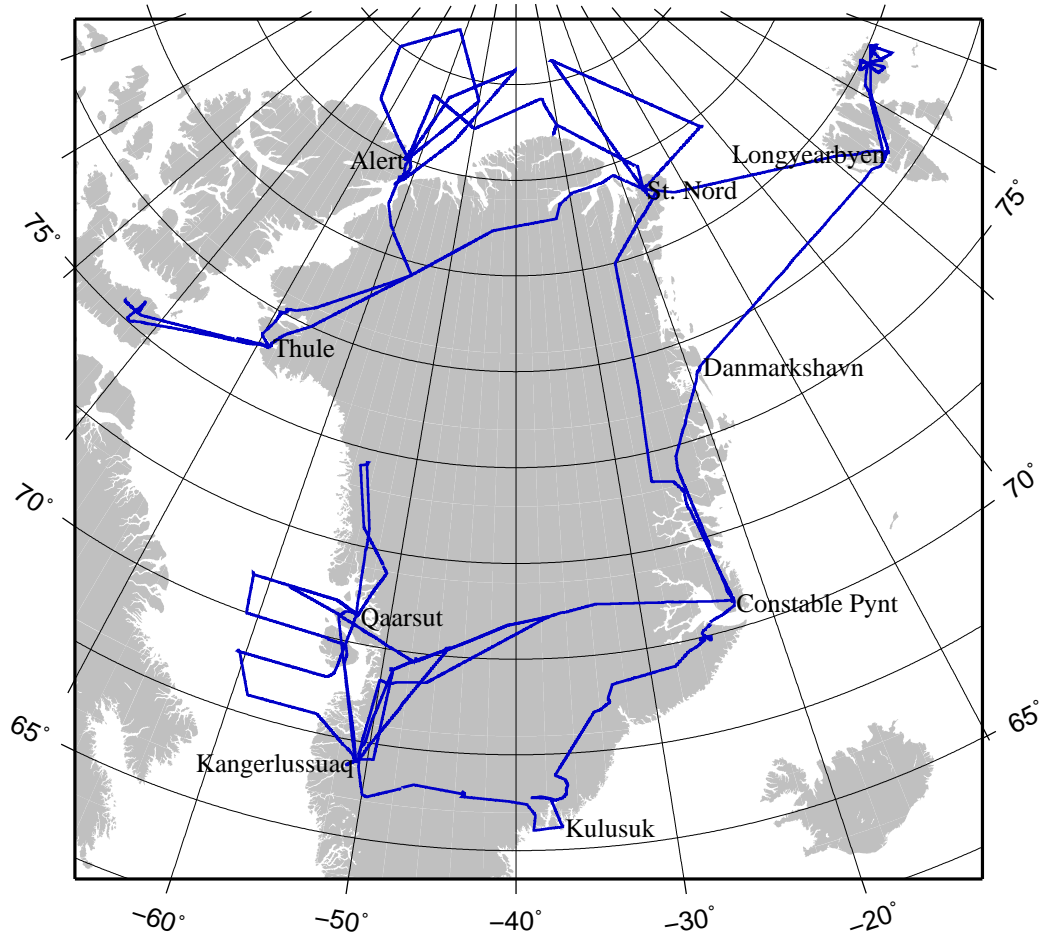


Figure 5: Tracks flown during CryoVEx 2006 by the Air Greenland Twin Otter equipped with the DNSC laser scanner system and the ASIRAS radar. (From Stenseng et al. (2007).)

The CryoVEx (CryoSat validation experiment) 2006 was carried out in spring 2006 as part of ESAs calibration and validation activities in preparation for CryoSat. The airborne campaign were carried out by the Danish National Space Center² took place between April 18th and May 19th and covered most of Greenland and surrounding sea-ice covered areas, see figure 5. The main objective of the campaign were to collect coincident laser and LAM radar measurements over predefined areas. Several ground teams operated in these areas to perform measurements of snow and ice properties and install radar corner reflectors.

A segment of high altitude mode ASIRAS data were collected on the 30th April following an ENVISAT ground track in the Fram Strait. This was on a request from ESA and this dataset is used for the work presented in this document. A detailed description of the campaign can be found in Stenseng et al. (2007).

²after a merge with the Technical University of Denmark in 2007, Danish National Space Center became a part of DTU-Space, National Space Institute

3.1 Hardware Installation

The ASIRAS instruments were installed in the Air Greenland owned Twin Otter OY-POF in a hangar in Kangerlussuaq, West Greenland. For the Twin Otter new antenna cables had to be made to accommodate the longer distance between the ASIRAS instrument and the ASIRAS antenna, compared with the Donier 228 used for the initial certification of the ASIRAS system. The ASIRAS antenna is mounted pointing 2° backwards to compensate for the average pitch of the aircraft during normal flight.

A sketch of approximate instrument positions can be found in figure 6 and pictures of the actual installation is shown in figure 7. Two GPS antennas is permanent installed on the OY-POF. During campaigns the antennas are connected to a series of GPS receivers and instruments, with embedded GPS receivers, through antenna splitters. This ensures that all measurement datetions is in the same time system (UTC)³. The front GPS antenna is placed over the left wing (behind the front operator seat) and the rear is placed above the laser/INS plate in the rear baggage compartment. After the post processing it is possible to link each measurement to an accurate position and describe the attitude of the aircraft during that measurement.

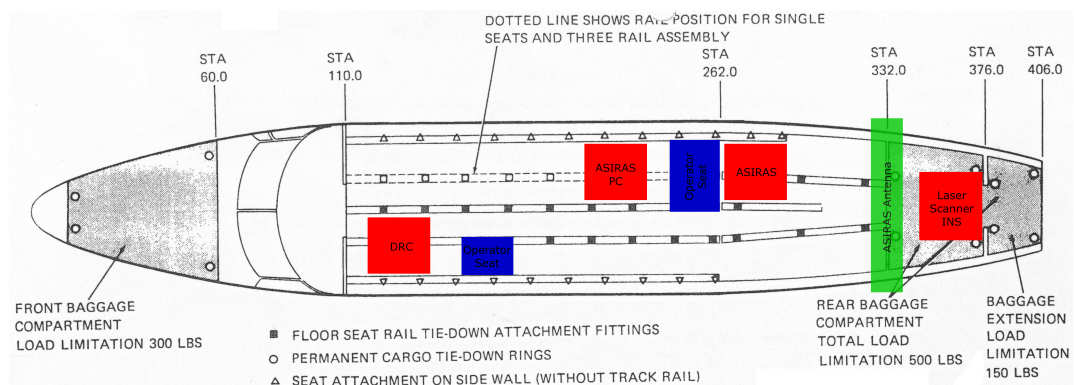


Figure 6: Sketch of approximate instrument positions. (From Stenseng et al. (2007).)

³GPS measurements are in GPS time frame which tied to UTC through an integer second offset.



(a) The ASIRAS control PC inside the cabin during survey.



(b) ASIRAS antenna mounted in front of the opening for the laser scanner.



(c) ASIRAS instrument installed in the rack with a GPS instrument (Trimble 4000).

Figure 7: Photos of the ASIRAS installation. (From Stenseng et al. (2007).)

4 ASIRAS HAM data over open ocean

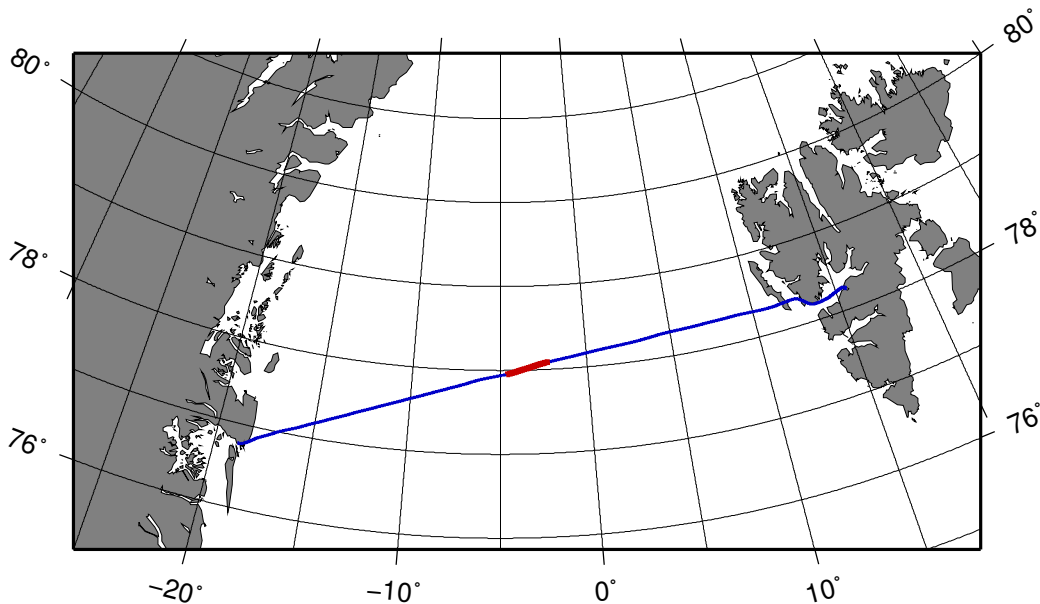


Figure 8: April 30 flight (blue) and profile where ASIRAS HAM data were collected (red).

One HAM profile over open ocean were collected during the CryoVEx 2006, see figure 8. The weather conditions during the flight were less optimal for radar data collection, but the flight were the only opportunity to collect the desired type of data. The profile were collected on April 30th 2006 between 10.08 and 10.23 UTC, following an Envisat track with a commanded collection of individual echoes. Unfortunately it has not been possible to get any data from the Envisat radar altimeter due to some error.

The ASIRAS processor has been updated several times since the profile were collected and processed for internal release. To obtain the stack data and benefit from the updates to the processor the profile has been reprocessed with the current version 4.02, and not the version 3.06, of the processor before any analysis.

The profile were processed with version 4.02 of the ASIRAS processor, with enabled diagnostic stack output. The resulting level 1b output were then compared with the level 1b output from version 3.06 of the processor, to ensure a general agreement between the two versions of the processor.

4.1 Typical waveforms

For the data acquisition ASIRAS were configured to 1 GHz bandwidth, 4 μ s pulse length and 2.5 kHz pulse repetition frequency. During the profile the aircraft speed were held between 69 m/s and 72 m/s with an average of 70.5 m/s, and the elevation above the ellipsoid between 2773 m and 2775 m with an average of 2774 m.

After processing the profile contains 7280 multi-looked waveforms. To ensure data of good quality and consistency, observations with antenna roll angle above ± 1.0 degree has been rejected. This meant that around half the waveforms has been rejected due to side

wind forcing the aircraft into an average roll of -0.9 degree. The remaining 3882 waveforms were visually inspected to identify typical waveforms, and key parameters like width and peak power were noted for a selection of each typical waveform. Based on an iterative adjustment of the found key parameters the waveforms were divided into three groups. The waveforms in each group are resampled and the 60% point of the leading edge are aligned to zero. Finally the mean and standard deviation of each resampled and aligned range bin is calculated and plotted, see figures 9, 10 and 11. The 60% point is equal to the retracked height given in the level 1b product and has been chosen for convenience, any arbitrary point on the leading edge could have been used. The 60% point is not a measure for the surface, but only valid as a common reference point for waveforms with similar shape.

4.1.1 Gaussian waveform

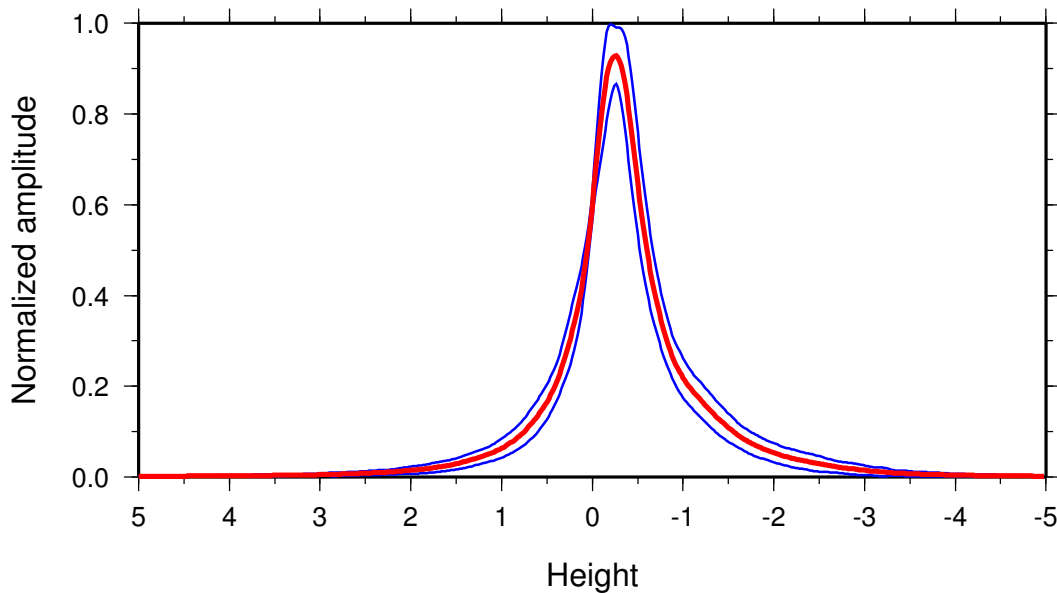


Figure 9: Gaussian mean waveform. The average waveform (red) plotted with the one σ (blue) standard deviation.

The first and, with only 151 waveforms, the least represented waveform type is the narrow Gaussian shaped waveforms. These waveforms are characterized by a narrow and almost symmetrical peak with relatively large peak power. The deviation between the individual waveforms in the group is small and part of the deviation in figure 9 could be caused by the resampling.

4.1.2 Skewed waveform

The most dominant waveform is a wider and slightly skewed version of the narrow Gaussian waveform. The 2605 waveforms in this group are in general less smooth and have a slightly lower peak power. The added noise compared to the Gaussian waveforms also give rise to a wider one σ standard deviation.

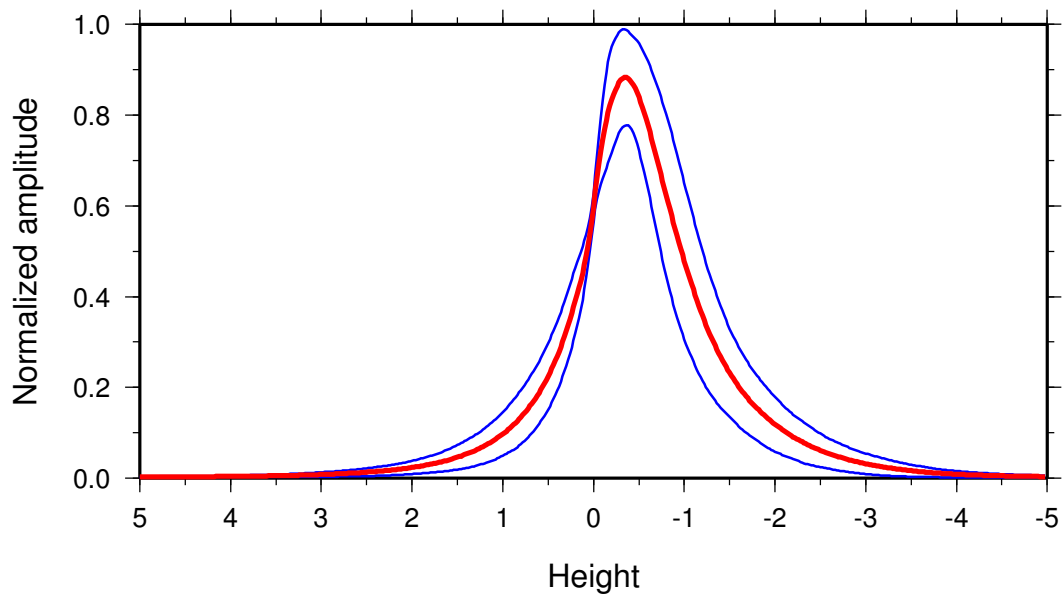


Figure 10: Skewed waveforms. The average waveform (red) plotted with the one σ (blue) standard deviation.

4.1.3 Waveform with tail

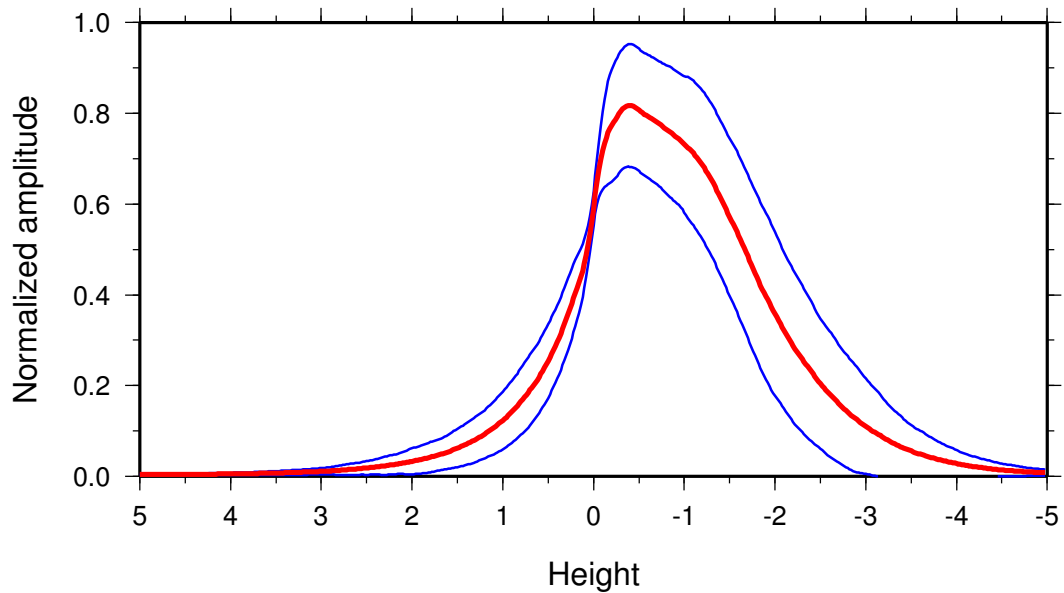


Figure 11: Waveforms with tail. The average waveform (red) plotted with the one σ (blue) standard deviation.

The remaining 1126 waveforms have a leading edge comparable to the skewed waveform but the trailing slope is longer.

The characteristics of the three mean waveforms are given in table 2. For this analysis the mean waveforms has been normalize to a max peak power of one. The slope of the leading edge is in this case defined as the slope of the best fitting straight line in the interval between 50% and 90% power. The length of the leading is defined as the distance between 10% and 90% power and width of top is defined as the part where the power is above 90%.

	Gaussian	Skewed	Tail
Number	151	2605	1126
Peak power [W]	$2.3 \cdot 10^{-2}$ – $5.5 \cdot 10^{-2}$	$1.2 \cdot 10^{-2}$ – $4.9 \cdot 10^{-2}$	$6.1 \cdot 10^{-3}$ – $4.9 \cdot 10^{-2}$
Slope of leading edge	2.1	1.6	1.4
Length of leading edge	0.92 m	1.2 m	1.4 m
Width of top	0.26 m	0.42 m	0.84 m
Length of trailing edge	1.2 m	1.6 m	2.3 m

Table 2: Comparison of waveforms.

4.2 Distribution of typical waveforms

The distribution of waveform of the tree groups has been investigated but no apparent pattern has been found. All types of waveforms are evenly distributed along the profile and the mean shape is close to constant throughout the profile.

Figure 12 show a section with 200 waveforms and their classification indicated by color code at the bottom. The only pattern seen in the distribution of the three types is a periodic shift between Gaussian and skewed waveforms on one side and tail waveforms on the other.

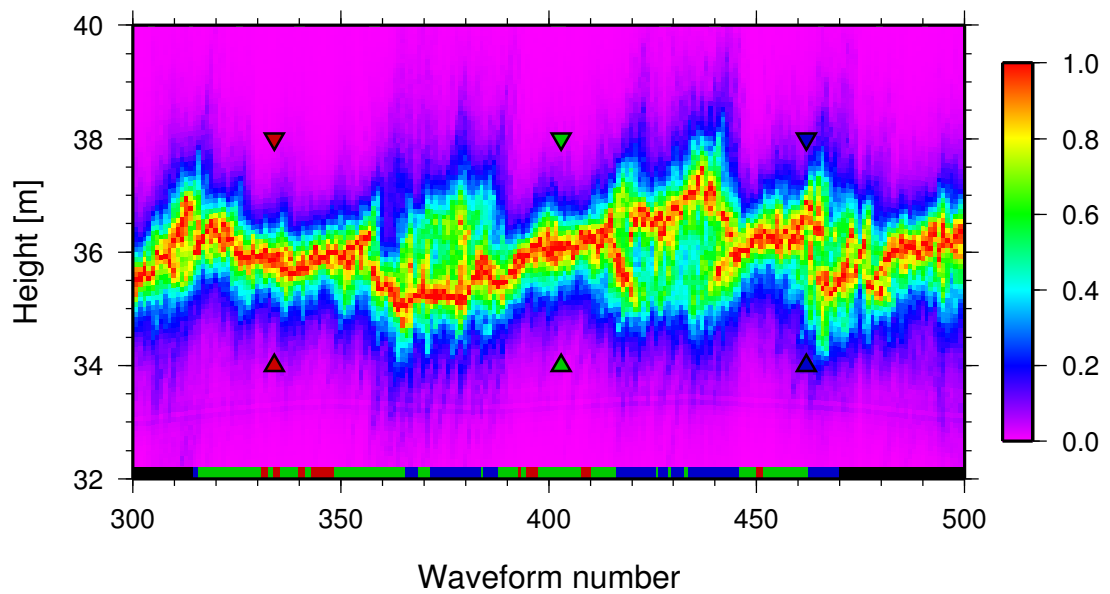


Figure 12: Distribution of the three typical waveform types. The bottom line is color coded after the classification; Gaussian (red), skewed (green), tail (blue), and rejected (black). The three waveforms marked with triangles are selected for further analysis.

5 Waveform stacks before multi-look

As described in Cullen (2007) (see also figure 4) it is possible to output the look stack before the summation. The ASIRAS instrument runs at a constant PRF and the short travel time associated with an airborne instrument allows each pulse to be transmitted and received before the next pulse is transmitted. Since all pulses are coherent it is possible to select the number of pulses in a burst during post processing.

Each burst is divided into a number of Doppler beams and beams that illuminate the current level 1b surface area are slant range corrected and summed to form the current level 1b waveform. Thus the number of beams that are summed to form one level 1b waveform depends on the range to the reflecting point and the speed of the aircraft. For the Fram Strait profile an average of 160 Doppler beams has been summed to form each level 1b waveform.

5.1 Examples of stacks

The profile has been re-processed, with a burst size of 128 pulses, to obtain the stack data and one representative waveform has been chosen for each of the three waveform types. Figures 13 to 15 show individual beams forming the final level 1b waveform. As expected the power is focused within a few range bins for the Gaussian and skewed waveforms but more spread for the waveform with tail, also the speckle noise is visible in all figures.

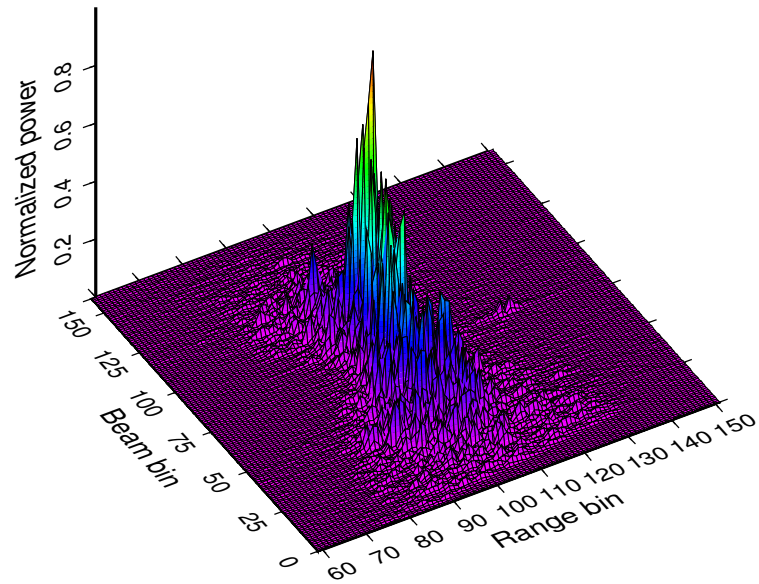
The effect of the slant range correction is clear in figure 13b, 14b, and 15b where the power is distributed along a hyperbolic band. Furthermore it is seen that after the slant range correction the first and last five to ten beams is out of range at the range of the scattering surface.

By close inspection of figure 13b, 14b, and 15b a attenuated hyperbola centered around beam bin 80 becomes visible, this is probably the effect of a DC component being removed by the processor. Finally beam bin 80 and 120, of the total 160 beams, have an apparent higher average power than the other beams, but the reason for this is unknown.

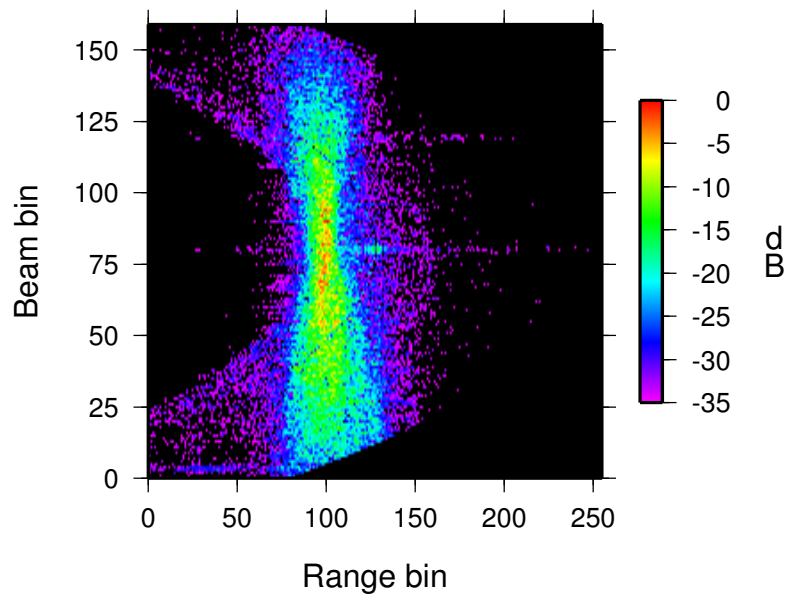
5.2 Power versus look angle

Figure 16 show the sum of power in each beam bin for the three stacks shown in figure 13 to 15. It is obvious that the top seems to be shifted between one and two degrees forward for all stacks, this is believed to be caused by the antenna not pointing nadir. The average pitch of the aircraft were around 3.5° , due to heavy cargo, during the profile and the antenna is tilted 2° backwards relative to the aircraft, see section 3.1, leaving the antenna pointing 1.5° forward.

A comparison between the summed power and an ideal two way antenna pattern, comparable to ASIRAS and shifted 1.5° forward, indicates that the returned power in the beams is limited primarily by the antenna pattern and in this case not the characteristics of the surface. This observation is not necessarily true for other surfaces or sea states.

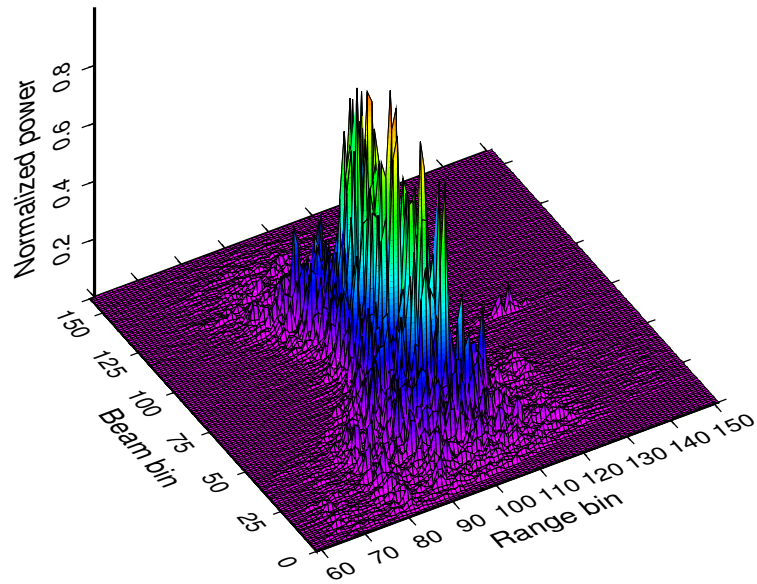


(a) Normalized power as function of beam and range bin.

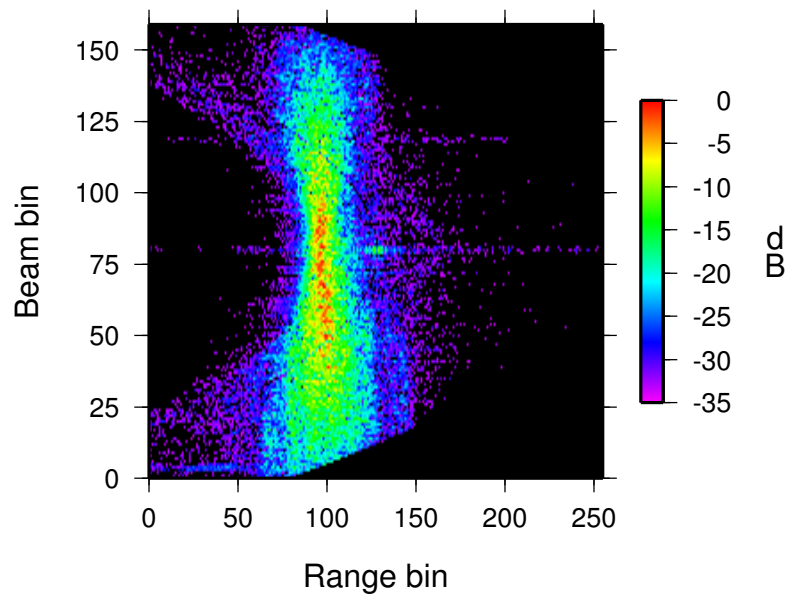


(b) Normalized power in dB as function of beam and range bin.

Figure 13: Selected waveform of Gaussian type.

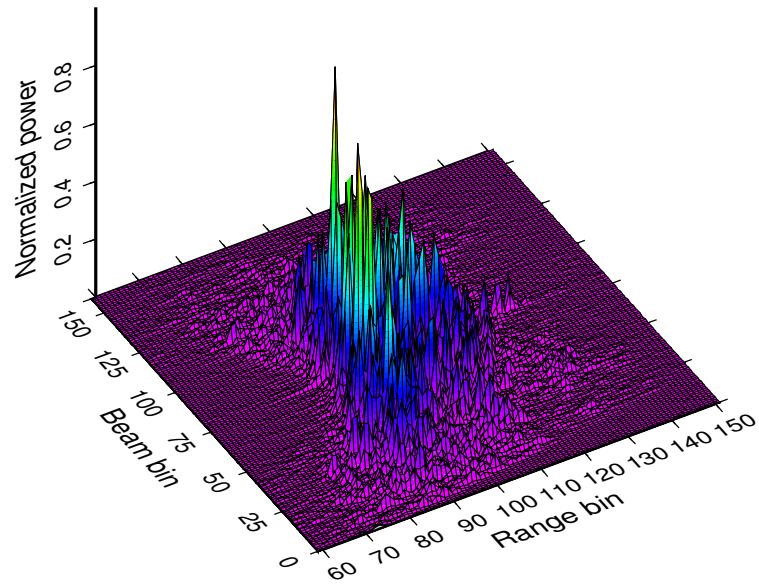


(a) Normalized power as function of beam and range bin.

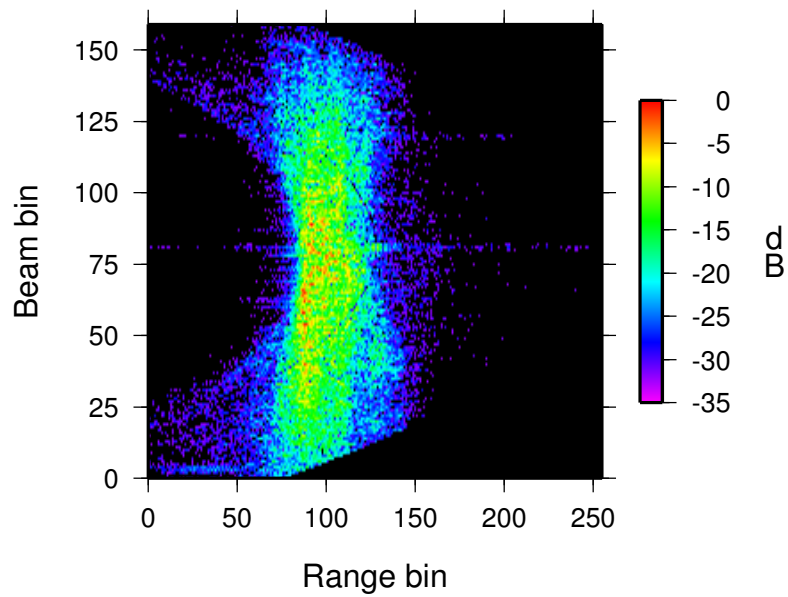


(b) Normalized power in dB as function of beam and range bin.

Figure 14: Skewed waveform stack.



(a) Normalized power as function of beam and range bin.



(b) Normalized power in dB as function of beam and range bin.

Figure 15: Waveform with tail stack.

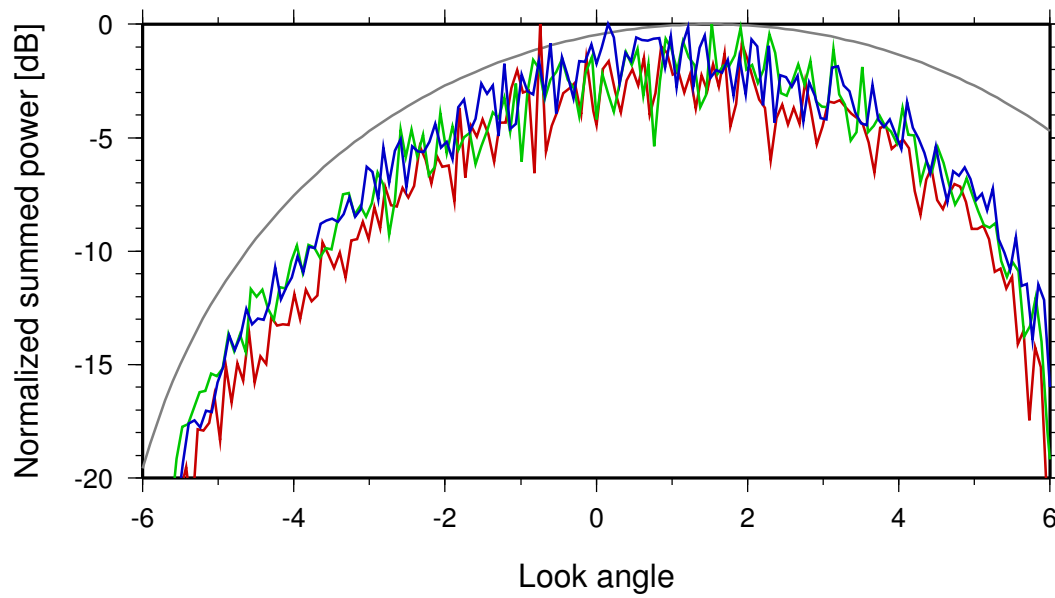


Figure 16: Summed power as a function of look angle for the each of the representative selected waveforms; Gaussian waveform (red), skewed waveform (green), and waveform with tail (blue). For comparison an ideal two way antenna pattern, comparable to ASIRAS and shifted 1.5° , is shown in gray.

6 Along-track beam selection

To ensure a reliable data collection over steep terrain it was decided to use a wide along-track antenna pattern thus making ASIRAS less sensitive to aircraft pitch maneuvers. The wide antenna pattern demands a high PRF to allow the Doppler spectrum of the main beam to be sampled unambiguously. The high PRF used by ASIRAS ensures a unambiguous sampling of the Doppler spectrum under normal flying conditions.

As the look angle increases the range between the lower and upper frequency limits of the Doppler bin also increases. At a critical angle (θ_c), when the range between the lower and upper frequency limits of the Doppler bin becomes comparable to the range resolution, the beams starts to degrade the resulting waveform. For a Doppler cell width ($x_{Doppler}$) much greater than the range resolution ($r_{resolution}$) the critical angle (θ_c) can be expressed as:

$$\theta_c < a \cdot \frac{r_{resolution}}{x_{Doppler}} \quad (1)$$

where a is a factor close to unity depending on the tolerance on the resulting waveform.

6.1 Comparison of full along-track beam summing and selected beam summing

The current standard processing sum all beams within the current level 1b surface area to form the level 1b waveform, which means that there is a risk that the level 1b waveforms is degraded by the inclusion of beams with a high look angle. A comparison between full along-track beam summing and selected beam summing has been performed to estimate the effect of the degradation associated with full along-track beam summing.

For the following investigation the three representative waveforms discussed in section 5.1 is used. For all three waveforms an angular cutoff of 1.4° , obtained from equation 1 where $r_{resolution} = 0.08783$ m, $x_{Doppler} = 3.6$ m and $a = 1$, has been used. All beams within the angular cutoff has been summed to form a waveform and compared with a waveform consisting of all beams illuminating the selected level 1b area. This reduces the number of beams in the resulting waveform from 160 beams to 37 beams.

In figures 17, 18 and 19 it is seen that the leading becomes much steeper and the leading toe almost disappears. For the Gaussian and skewed waveform the tail is also significant smaller, whereas the tail on the waveform with tail seems more wiggly. Overall all three waveforms is greatly enhanced by only selecting the near nadir beams.

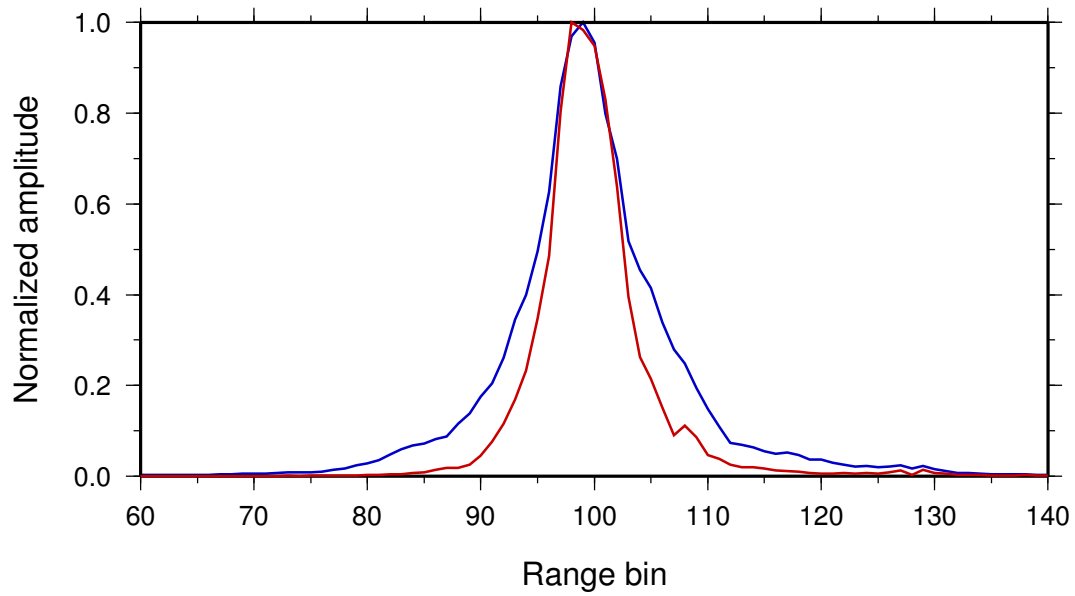


Figure 17: Comparison of full along-track beam summing (blue) and selected beam sum (red) for a Gaussian waveform.

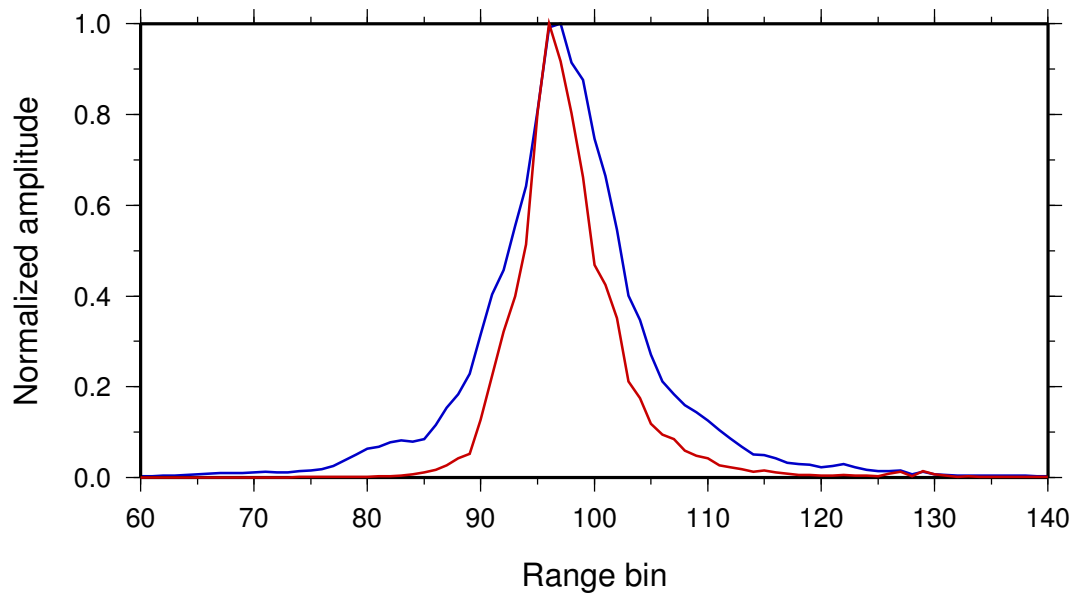


Figure 18: Comparison of full along-track beam summing (blue) and selected beam sum (red) for a skewed waveform.

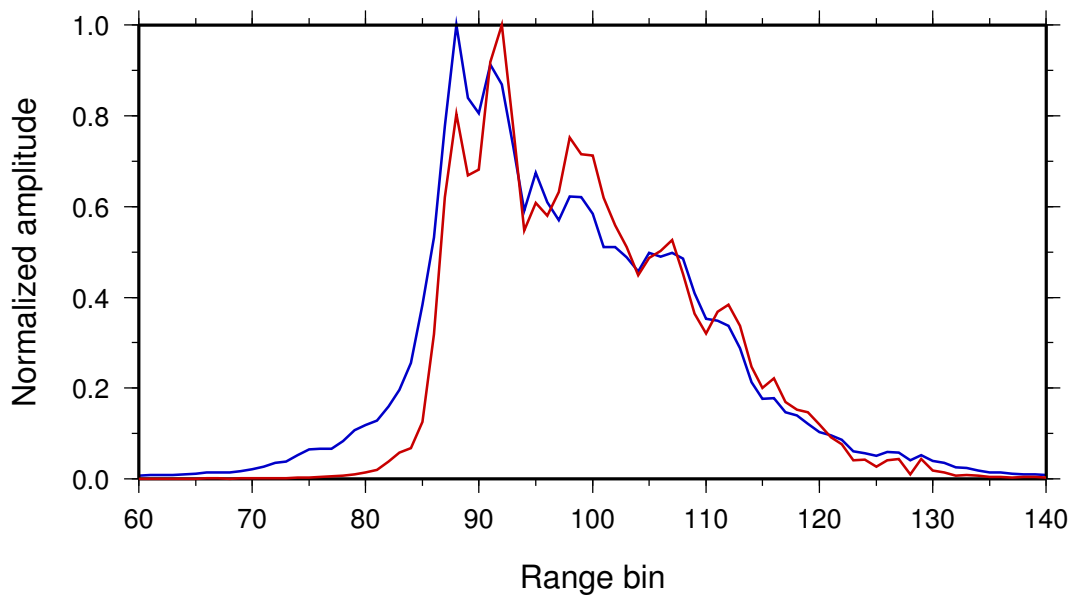


Figure 19: Comparison of full along-track beam summing (blue) and selected beam sum (red) for a waveform with tail.

7 Guideline for future campaigns

During the analysis of the profile no major, but two minor, issues has been found. Both minor issues are regarding the attitude of the aircraft during data collection, and thus the orientation of the antenna relative to the scattering surface. Approximate half the waveforms have been rejected due to roll maneuvers greater than $\pm 1^\circ$ and heavy loading of the aircraft lowered the tail resulting in a 1.5° forward pointing antenna.

- Pilots should be briefed about the sensitivity of the orientation of the antenna with respect to the scattering surface, and possibilities to avoid roll maneuvers should be discussed.
- Transit flights over ocean should be planned as straight and HAM data should be acquired during that period.
- Transit flights over land should allow data collection over inland waters if possible.
- The data collection should cover the transition between land and ocean when possible.
- Ground tracks and timing for Envisat (and CryoSat-2 when launched) during the entire field period should be obtained to allow opportunity under-flight.
- Processing should be optimized to reject beams far from nadir.

For high altitude mode the data rate is approximately 10 Gb/hour making the added data volume, associated with the ocean oriented data collection, acceptable for field work.

8 Conclusion

The work presented in this technical note has described the properties of an ASIRAS high altitude mode profile collected over the Fram Strait. The profile has undergone an empirical analysis where three typical level 1b waveform types have been identified and described. The occurrence and distribution of the three waveform types have no obvious pattern, except a periodic shift between groups of Gaussian and skewed waveforms and groups of tail waveforms.

The stacks from one representative level 1b waveform of each typical type has investigated to determine the power content as a function of the look angle. This investigation revealed that the look angle power is closely related to the antenna pattern and that the antenna was pointing off nadir during the profile.

It has been shown that the level 1b waveforms can be enhanced by a carefully selecting the Doppler beams that are summed, instead of using all Doppler beams that illuminate the level 1b area.

Finally a short guideline for future ASIRAS campaigns has been presented.

References

- Cullen, R. (2007). *ASIRAS, Product Description, Issue: 2.5*. European Space Agency, 2.5.
- Cullen, R. A. and Wingham, D. J. (2002). Cryosat level 1b processing algorithms and simulation results. In *Geoscience and Remote Sensing Symposium, 2002. IGARSS '02. 2002 IEEE International*, volume 3, pages 1762–1764. Centre for Polar Obs. & Modelling, Univ. Coll. London, UK, IEEE.
- ESA, editor (2007). *ESA's CryoSat-2 Multi-Mode Level 0 to Level 1b Science Processors—Algorithm Design and Pre-Launch Verification with ASIRAS*. Envisat Symposium 2007.
- Lentz, H., Braun, H.-M., Younis, M., Fischer, C., Wiesbeck, W., and Mavrocordatos, C. (2002). Concept and realization of an airborne sar/interferometric radar altimeter system (asiras). *IEEE International Geoscience and Remote Sensing Symposium*, 6:3099–3101 vol.6.
- MacArthur, J. (1976). Design of the seasat-a radar altimeter. *OCEANS*, 8:222–229.
- Mavrocordatos, C., Attema, E., Davidson, M., Lentz, H., and Nixdorf, U. (2004). Development of asiras (airborne sar/interferometric altimeter system). pages 2465–2467.
- Raney, R. (1998). The delay/doppler radar altimeter. *IEEE Transactions on Geoscience and Remote Sensing*, 36(5):1578–1588.
- RST (2007). *ASIRAS Design Description*. RST Radar Systemtechnik AG, 2 edition.
- Stenseng, L., Hvidegaard, S. M., Skourup, H., Forsberg, R., Andersen, C. J., Hanson, S., Cullen, R., and Helm, V. (2007). Airborne lidar and radar measurements in and around Greenland, CryoVEx 2006. Technical Report 9, Danish National Space Center.
- Wingham, D. J., Francis, C. R., Baker, S., Bouzinac, C., Brockley, D., Cullen, R., de Chateau-Thierry, P., Laxon, S. W., Mallow, U., Mavrocordatos, C., Phalippou, L., Ratier, G., Rey, L., Rostan, F., Viau, P., and Wallis, D. W. (2006). Cryosat: A mission to determine the fluctuations in earth's land and marine ice fields. *Advances in Space Research*, 37:841–871.